



Revised Properties and Dynamical History for the HD 17156 System

Stephen R. Kane¹, Michelle L. Hill¹, Paul A. Dalba^{2,3,10}, Tara Fetherolf^{1,11}, Gregory W. Henry⁴, Sergio B. Fajardo-Acosta⁵, Crystal L. Gnilk⁶, Andrew W. Howard⁷, Steve B. Howell⁶, and Howard Isaacson^{8,9}

¹Department of Earth and Planetary Sciences, University of California, Riverside, CA 92521, USA; skane@ucr.edu

²Department of Astronomy and Astrophysics, University of California, Santa Cruz, CA 95064, USA

³SETI Institute, Carl Sagan Center, 339 Bernardo Ave, Suite 200, Mountain View, CA 94043, USA

⁴Center of Excellence in Information Systems, Tennessee State University, Nashville, TN 37209, USA

⁵Caltech/IPAC, Mail Code 100-22, Pasadena, CA 91125, USA

⁶NASA Ames Research Center, Moffett Field, CA 94035, USA

⁷Department of Astronomy, California Institute of Technology, Pasadena, CA 91125, USA

⁸Department of Astronomy, University of California, Berkeley, CA 94720, USA

⁹Centre for Astrophysics, University of Southern Queensland, Toowoomba, QLD 4350, Australia

Received 2023 March 16; revised 2023 April 24; accepted 2023 April 28; published 2023 May 25

Abstract

From the thousands of known exoplanets, those that transit bright host stars provide the greatest accessibility toward detailed system characterization. The first known such planets were generally discovered using the radial-velocity technique, then later found to transit. HD 17156b is particularly notable among these initial discoveries because it diverged from the typical hot-Jupiter population, occupying a 21.2 day eccentric ($e = 0.68$) orbit, offering preliminary insights into the evolution of planets in extreme orbits. Here we present new data for this system, including ground- and space-based photometry, radial velocities, and speckle imaging, that further constrain the system properties and stellar/planetary multiplicity. These data include photometry from the Transiting Exoplanet Survey Satellite that cover five transits of the known planet. We show that the system does not harbor any additional giant planets interior to 10 au. The lack of stellar companions and the age of the system indicate that the eccentricity of the known planet may have resulted from a previous planet–planet scattering event. We provide the results from dynamical simulations that suggest possible properties of an additional planet that culminated in ejection from the system, leaving a legacy of the observed high eccentricity for HD 17156b.

Unified Astronomy Thesaurus concepts: [Exoplanet astronomy \(486\)](#); [Exoplanet dynamics \(490\)](#); [Exoplanet detection methods \(489\)](#); [Exoplanet systems \(484\)](#); [Exoplanets \(498\)](#); [Radial velocity \(1332\)](#); [Photometry \(1234\)](#)

Supporting material: machine-readable table

1. Introduction

The large number of exoplanet discoveries have uncovered a diverse range of planetary architectures, many of which differ significantly from the planets and orbits found in the solar system (Ford 2014; Winn & Fabrycky 2015; Kane et al. 2021a). One of the more extreme divergences from the solar system architecture is that of highly-eccentric giant planets within the broader eccentricity distribution (Shen & Turner 2008; Kane et al. 2012; Van Eylen & Albrecht 2015). The existence of eccentric giant planets may be the result of disk interactions during formation (Clement et al. 2021) or may reveal a potentially dynamically turbulent past regarding planet–planet scattering events (Chatterjee et al. 2008; Ford & Rasio 2008; Kane & Raymond 2014; Carrera et al. 2019). Such planets are extremely important with respect to the evolution of planetary system dynamics (Jurić & Tremaine 2008; Ford 2014; Winn & Fabrycky 2015), including the possible locations of potentially habitable terrestrial planets in the system (Kane & Gelino 2012; Georgakarakos et al. 2018; Hill et al. 2018; Sánchez et al. 2018; Kane & Blunt 2019).

Highly-eccentric planets also provide opportunities to study atmospheric circulation and radiative forcing in extreme flux environments (Kane & Gelino 2011; Kataria et al. 2013; Lewis et al. 2013). Eccentric planets that transit their host star are therefore particularly valuable assets in the exoplanet inventory since they reveal mass–radius relations and atmospheric information via transmission spectroscopy (Kane & von Braun 2009; Mayorga et al. 2021). Fortunately, eccentric planets also have an enhanced transit probability (Barnes 2007; Burke 2008; Kane & von Braun 2008), resulting in several key discoveries of long-period transiting planets in eccentric orbits, such as HD 80606b (Naef et al. 2001; Laughlin et al. 2009; de Wit et al. 2016), and the more recent case of Kepler-1704b (Dalba et al. 2021).

Among the early detection of planetary transits, the most significant were those planets discovered with the radial velocity (RV) method, due to the relative brightness of their host stars (Kane 2007; Kane et al. 2009). The Transiting Exoplanet Survey Satellite (TESS) has carried out photometric monitoring of bright stars throughout the sky since its launch in 2018 (Ricker et al. 2015), including many known RV exoplanet host stars (Dalba et al. 2019; Kane et al. 2021b). These TESS observations have enabled the detection of transits for several systems, including HD 118203 (Pepper et al. 2020) and HD 136352 (Kane et al. 2020). Prior to the launch of the Kepler mission, the limited group of RV transiting planets included the very first detected transiting planet; HD 209458b (Charbonneau et al. 2000; Henry et al. 2000). A significant

¹⁰ Heising-Simons 51 Pegasi b Postdoctoral Fellow.

¹¹ UC Chancellor’s Fellow.



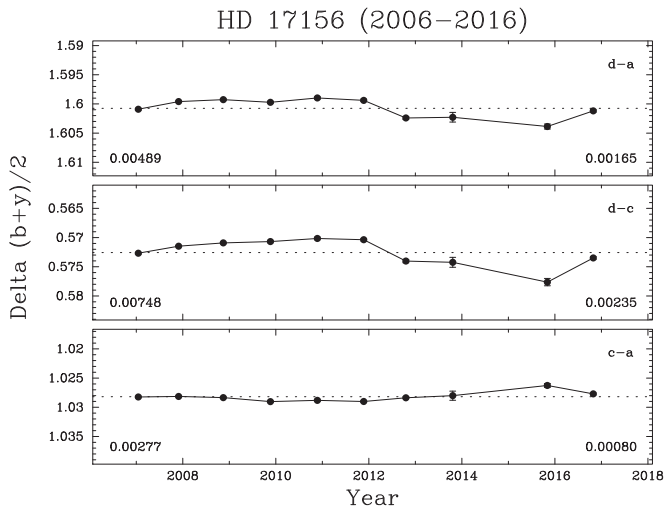


Figure 1. Comparison of the seasonal means of the d-a, d-c, and c-a differential magnitudes show that the observed variability is intrinsic to HD 17156.

milestone planet is HD 17156b, a Jovian-mass planet discovered via RVs by Fischer et al. (2007) and then subsequently found to transit the host star by Barbieri et al. (2007). The high interest in the planet stemmed largely from the divergence from previous hot-Jupiter discoveries, both in terms of its relatively large orbital period ($P = 21.2$ days) and eccentricity ($e = 0.68$). The interest in the system resulted in numerous follow-up observations to refine the system parameters, including the planet size/mass and orbit (Gillon et al. 2008; Irwin et al. 2008; Barbieri et al. 2009; Winn et al. 2009; Dawson & Johnson 2012) and space-based observations to characterize the host star and star–planet interactions (Gilliland et al. 2011; Nutzman et al. 2011; Southworth 2011; Maggio et al. 2015). The HD 17156 system was also intensively studied with respect to the potential misalignment between the planetary orbital axis and the stellar rotational axis via detection of the Rossiter–McLaughlin (R-M) effect. The spin–orbit was initially found to exhibit substantial misalignment (Narita et al. 2008), but further observations indicated that the spin–orbit misalignment was small (Cochran et al. 2008; Narita et al. 2009). With all of these follow-up observations, the HD 17156 system remains a crucial milestone in our knowledge of eccentric orbits, giant-planet formation and evolution, and orbital dynamics within planetary systems.

In this paper, we present new observations of HD 17156, including ground-based photometry to measure the long-term stellar variability, TESS photometry that reveals five transits of the known exoplanet, new RV data that updates the orbit, and speckle imaging to constrain the presence of stellar companions. These observations improve the mass, radius, and orbit of the planet, and provide insight into the dynamical history of the planet. Section 2 describes the data sources for the photometric, RV, and imaging components of the observations. Section 3 presents the results from the data analysis, including revised properties for both the star and planet, and constraints on additional bodies within the system. We discuss the implications of our data and analysis for the dynamical history of the planet in Section 4, then provide concluding remarks and suggestions for further work in Section 5.

Table 1
Summary of T12 APT Photometric Observations for HD 17156

Observing Season	N_{obs}	Date Range (HJD – 2400000)	Sigma (mag)	Seasonal Mean (mag)
2006–07	214	54001–54179	0.00212	1.08680(15)
2007–08	400	54370–54535	0.00183	1.08554(09)
2008–09	124	54728–54881	0.00146	1.08509(13)
2009–10	64	55092–55245	0.00141	1.08520(18)
2010–11	69	55463–55610	0.00160	1.08457(19)
2011–12	64	55823–55971	0.00154	1.08488(19)
2012–13	35	56186–56265	0.00148	1.08821(25)
2013–14	12	56558–56634	0.00259	1.08826(75)
2014–15	0
2015–16	33	57293–57377	0.00294	1.09075(51)
2016–17	44	57666–57734	0.00134	1.08734(20)

2. Observations

Due to the long-standing interest in HD 17156 (HIP 13192, TIC 302773669, TOI-1573), the star has been observed on numerous occasions. Here, we describe observations carried out for this project, combining space- and ground-based photometry, additional RVs, and speckle imaging.

2.1. Photometry

2.1.1. T12 APT

We acquired 1059 out-of-transit photometric observations of HD 17156 over 10 observing seasons from 2006–07 to 2016–17. The data were acquired with the T12 0.80 m automatic photoelectric telescope (APT) at Fairborn Observatory in Arizona. The T12 APT has a dual channel photometer equipped with two EMI 9124QB photomultiplier tubes to measure differential magnitudes simultaneously in the Strömgren b and y passbands. To improve the photometric precision of the individual nightly observations, we combine the differential b and y magnitudes into a single $(b+y)/2$ “passband.” The precision of a single observation with T12, as measured from pairs of constant comparison stars, is typically around 0.0015–0.0020 mag on good nights. The T12 APT is functionally identical to the T8 APT, described in detail by Henry (1999).

The comparison stars were HD 15784 (star a), HD 19016 (star b), HD 16066 (star c), with HD 17156 designated as star d. Intercomparison of the six combinations of differential magnitudes (d-a, d-b, d-c, c-a, c-b, b-a) shows that star b is a low-amplitude variable, while stars a and c are constant to the limit of our precision. Therefore, we created differential magnitudes in the sense HD 17156 minus the mean brightness of HD 15784 and HD 16066 in the combined $(b+y)/2$ passband. Figure 1 plots the seasonal mean differential magnitudes of d-a, d-c, and c-a in the top, middle, and bottom panels, respectively. The numbers in the lower right of each panel are the standard deviations of the mean magnitudes from the mean of the mean magnitudes, represented by the dotted line in each panel. The numbers in the lower left give the total range in the seasonal means. Comparison of the three panels shows that most of the variability detected in these three stars is intrinsic to HD 17156.

Table 1 summarizes the observations of the d-ac differential magnitudes of HD 17156. Most standard deviations of the nightly observations from their individual seasonal means

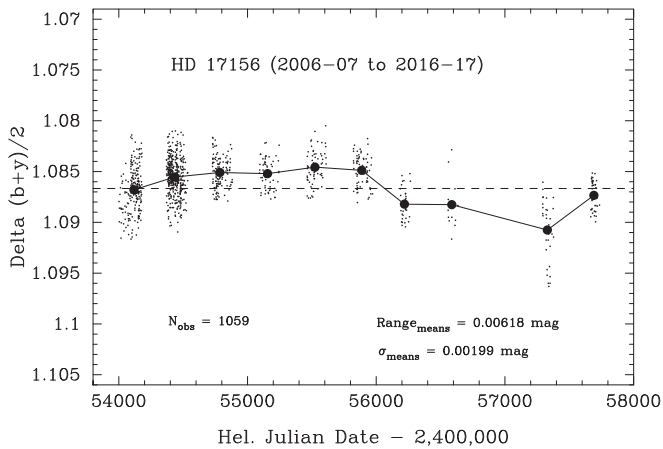


Figure 2. Nightly Strömgren $(b + y)/2$ band photometry of HD 17156 from 10 observing seasons from 2006–07 to 2016–17 (small circles), acquired with the T12 0.80 m APT at Fairborn Observatory. The star is constant from night-to-night within most observing seasons to the limit of our precision. The seasonal mean magnitudes are plotted as the large filled circles and cover a range of 0.00618 mag with a standard deviation from the mean of the seasonal means of 0.00199 mag, indicating low-amplitude year-to-year variability in HD 17156. The seasonal means suggest a stellar cycle of around 10 yr.

(column 4) fall between 0.00134 and 0.00212 mag, so the night-to-night scatter in the observations is similar to the typical measurement uncertainty. Table 1 also lists the 10 seasonal means (column 5), along with the last two digits of their standard deviations. The seasonal means cover a range of 0.00618 mag.

Analysis of the nightly d-ac differential magnitudes finds no significant periodicity between 1 and 100 days within any of the 10 individual observing seasons or in the data set as a whole. In particular, we find no evidence for periodicity around the estimated 17.8 day rotation period discussed in Section 3.1. Therefore, rotational modulation in the brightness of HD 17156 due to star spots is undetectable in our photometric observations. Furthermore, we find no significant variability at or around the 21.2 day period of the known planet, providing further evidence that the RV variations are due to the planetary reflex motion of the star.

Figure 2 plots the individual nightly differential magnitudes from the 10 observing seasons as small filled circles. The seasonal means are plotted as the large filled circles. The standard deviations of the individual seasonal means (see Table 1) are roughly the size of the plot symbols. The standard deviation of the individual mean magnitudes from their grand mean is 0.00199 mag, which is several times larger than the standard deviation of the individual means. The mean magnitudes in Figure 2 suggest a stellar cycle in HD 17156 of ~ 10 yr.

2.1.2. TESS

The TESS spacecraft observed HD 17156 during Sector 18 (2019 November 2 to 2019 November 27, in cycle 2), Sector 19 (2019 November 27 to 2019 December 24, in cycle 2), Sector 25 (2020 May 13 to 2020 June 8, in cycle 2), and Sector 52 (2022 May 18 to 2022 June 13, in cycle 4). These TESS data can be found in MAST¹². HD 17156 is relatively bright ($V \sim 8.2$) and so was observed with 2 minute cadence, compared to the 30 minutes sampling for most of the sky.

Since the orbital period of HD 17156b ($P = 21.2$ days) is less than the typical dwell time for TESS on a given sector, a transit event is all but guaranteed during a particular sector. Indeed, a single transit was detected in each of the Sectors 18, 19, and 25, and two transits were observed during Sector 52. The transits were easily detected by the Science Processing Operations Center pipeline, so HD 17156 was assigned TESS Object of Interest (TOI) number 1573.

Prior to our transit analysis, we investigated the variability of HD 17156 using the methodology described in Fetherolf et al. (2022). In brief, a Lomb–Scargle (LS; Lomb 1976; Scargle 1982) periodogram search from 1 to 13 days was performed on each sector of the 2 minute cadence Pre-search Data Conditioning (PDC) photometry acquired by TESS. A careful vetting process for determining significant periodic stellar variability and excluding systematic aliases was performed by Fetherolf et al. (2022), and the resulting variability catalog does not include HD 17156. Figure 3 shows the light curve (left), LS periodogram (center), and phase-folded light curve (right) for each TESS sector of photometry available for HD 17156 at the time of writing. The detected periodic signatures are inconsistent between TESS sectors and none of the LS periodograms reach a high-significance threshold of 0.1 normalized power. The most significant periodicity is Sector 18 (0.08 normalized power), but the periodogram is clearly biased toward upwards and downwards trends that occur near the spacecraft’s data uplink times. Therefore, we consider HD 17156 to be a relatively quiet, nonvariable star on timescales of < 13 days, in agreement with the APT results described in Section 2.1.1.

In preparation for the transit analysis, the TESS data were detrended for stellar variability and instrumental effects through the use of the keplersplinev2¹³ tool (Vanderburg & Johnson 2014). The analysis of the planetary signatures in these data are described in Section 3.

2.2. Radial Velocities

HD 17156 has been observed using the HIRES echelle spectrometer (Vogt et al. 1994) on the 10 m Keck I telescope since early 2006. The continued observations occurred within the framework of the California Legacy Survey, described in more detail by Fulton et al. (2021) and Rosenthal et al. (2021, 2022). The Keck RV measurements were created from observations with an iodine cell, producing a dense set of molecular absorption lines imprinted on the stellar spectra that enable robust wavelength calibration from which precision Doppler measurements and instrumental profile constraints are produced (Marcy & Butler 1992; Valenti et al. 1995). The Doppler shift for each star-times-iodine spectrum were extracted using the modeling techniques described by Butler et al. (1996), Howard et al. (2009). A subset of the RV data, including times of observation, relative RVs, and associated errors for the Keck data, are shown in Table 2. In total, 71 RV measurements are included in our full data set that span a period of ~ 17 yr, with a median uncertainty of 1.415 m s^{-1} . Note that there are other RV data sources that focus on the specific orbital location of inferior conjunction for the purpose of detecting the R-M effect (Cochran et al. 2008; Narita et al. 2008, 2009). However, those data are not included in this analysis as we found that they do not contribute significantly to

¹² DOI: [10.17909/t9-nmc8-f686](https://doi.org/10.17909/t9-nmc8-f686).

¹³ <https://github.com/avanderburg/keplersplinev2>

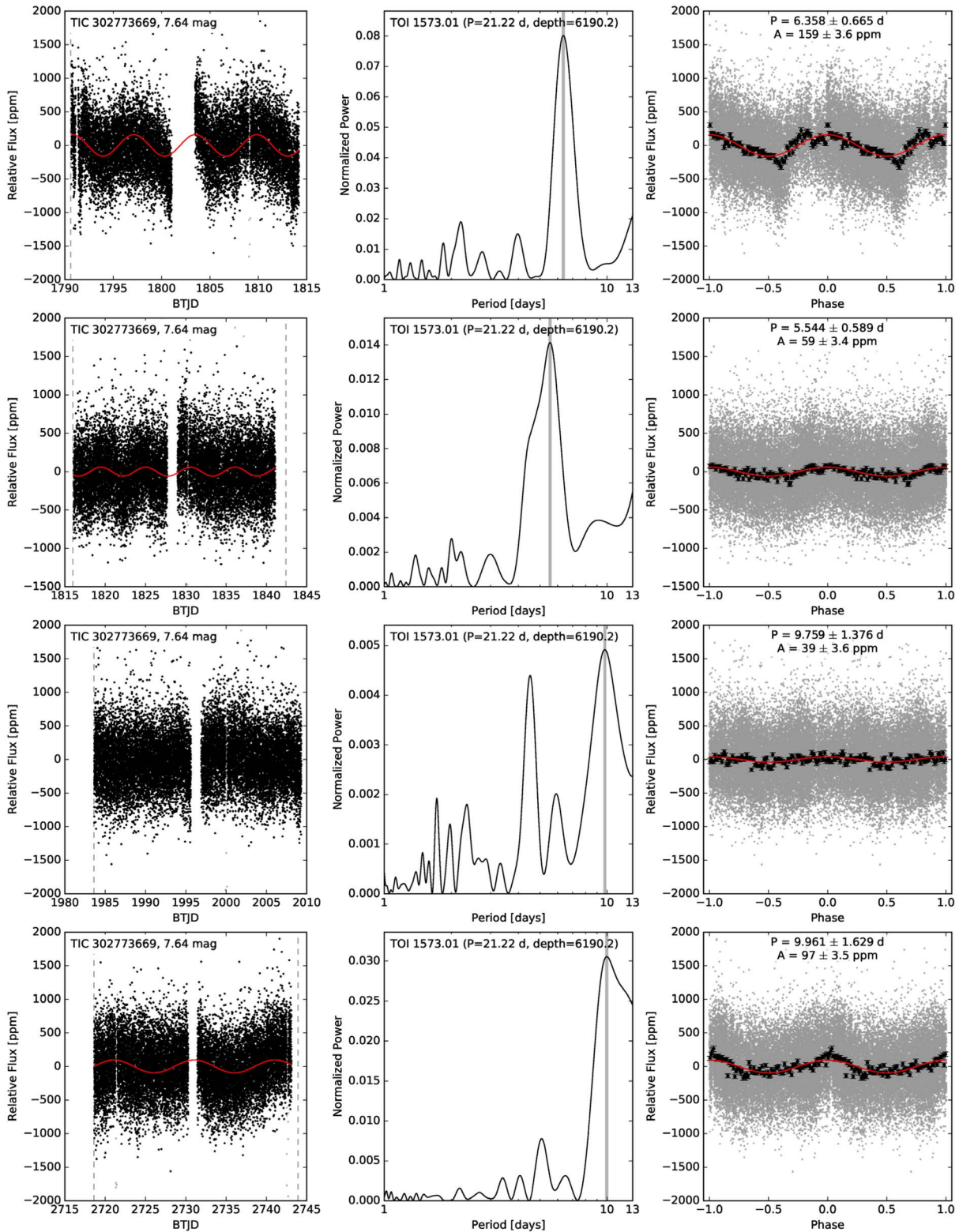


Figure 3. The TESS 2 minute PDC light curves (left), LS periodograms (center), and phase-folded light curves (right) from the variability analysis for HD 17156. Dates in the left panel are shown in Barycentric TESS Julian Date. The variability analysis is performed separately on each TESS sector, which is ordered in time from top to bottom: Sectors 18, 19, 25, and 52. The mean out-of-transit photometric scatter over all sectors is 380 ppm. The red curve shows a sinusoidal fit to the most significant periodicity. The gray points in the left panel indicate data that were removed from the variability analysis, which includes data flagged as poor quality, 5σ outliers, and transits of HD 17156b. In the right panel, the gray points indicate all data included in the variability analysis and the black points represent the binned data. The periodic signals detected by the LS periodograms are inconsistent between sectors and are low in normalized power (<0.1), such that we consider HD 17156 to be a quiet, nonvariable star on timescales <13 days.

Table 2
HD 17156 Radial Velocities

Date (BJD—2450000)	RV (m s ⁻¹)	σ (m s ⁻¹)
3746.7593	-15.279	1.639
3748.8014	31.516	1.776
3749.7980	42.631	1.780
3750.8048	63.699	1.569
3775.7800	130.727	1.784
3776.8097	150.371	1.628
3779.8306	133.042	1.563
3959.1318	-5.680	1.415
3962.0700	47.436	1.210
3963.1059	62.608	1.586
3964.1310	92.630	1.532
3982.0333	29.756	1.074
3983.0868	41.970	1.544
3983.9959	61.650	1.243
3985.0096	85.931	1.512
4023.9553	5.941	1.834
4047.9618	62.277	1.799
4083.9073	-69.172	1.226
4084.8328	-38.746	1.396
4085.8695	-20.385	1.650
4129.9276	9.324	1.401
4130.7326	30.847	1.451
4131.8572	43.177	1.900
4138.7692	162.379	1.311
4319.1285	-18.306	1.146
4336.0806	-156.118	1.169
4337.1220	-117.681	1.357
4339.1313	-47.422	1.196
4427.8273	31.948	1.419
4428.8656	51.232	1.529
4545.7235	-361.921	1.387
4545.7276	-364.986	1.285
4546.8283	-254.029	1.481
4546.8339	-254.519	1.435
4673.1254	-356.450	1.251
4702.1282	8.626	1.095
4703.0358	27.300	1.101
4704.1246	41.815	1.172
4705.0540	60.832	1.227

Note. The full data set is available online.

(This table is available in its entirety in machine-readable form.)

the overall Keplerian orbital fit, which is dominated by the long-term nature of the Keck/HIRES data.

2.3. Speckle Imaging

If a star hosting a planet candidate has a close bound companion (or companions), the companion can create a false-positive exoplanet detection if it is an eclipsing binary. Additionally, flux from the additional source(s) can lead to an underestimated planetary radius if not accounted for in the transit model (Ciardi et al. 2015; Matson et al. 2018). In order to ascertain the possibility of close, low-mass stellar companions to HD 17156, we conducted observations using the 'Alopeke instrument at the Gemini North Observatory (Scott et al. 2021). 'Alopeke provides simultaneous speckle imaging in two bands (562 and 832 nm) with output data products including a reconstructed image and robust contrast limits on

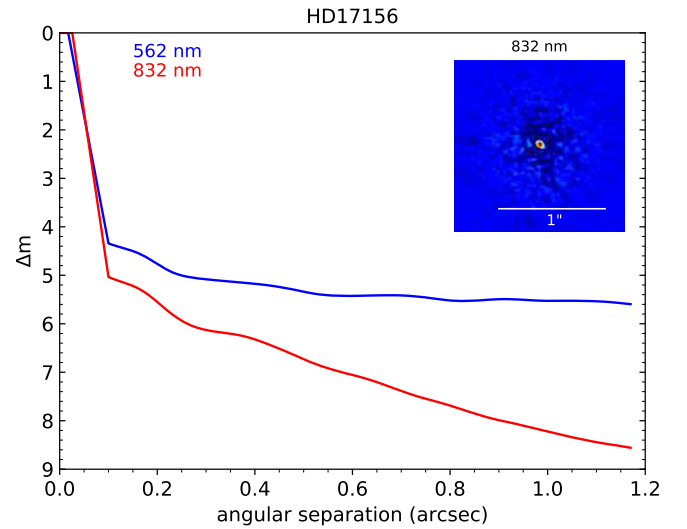


Figure 4. The 562 nm (blue) and 832 nm (red) contrast curve results and reconstructed speckle image for HD 17156, from observations carried out using the 'Alopeke instrument at the Gemini North Observatory.

Table 3
HD 17156 Derived Stellar Parameters

Parameter	Units	Values
M_*	Mass (M_\odot)	$1.285^{+0.064}_{-0.062}$
R_*	Radius (R_\odot)	$1.517^{+0.038}_{-0.036}$
L_*	Luminosity (L_\odot)	$2.76^{+0.19}_{-0.13}$
F_{Bol}	Bolometric flux (cgs)	$0.00000001477^{+0.000000000100}_{-0.000000000071}$
ρ_*	Density (cgs)	$0.517^{+0.039}_{-0.035}$
$\log g$	Surface gravity (cgs)	4.184 ± 0.024
T_{eff}	Effective temperature (K)	6046^{+76}_{-72}
[Fe/H]	Metallicity (dex)	0.208 ± 0.058
Age	Age (Gyr)	$3.3^{+1.2}_{-1.0}$
A_V	V-band extinction (mag)	$0.090^{+0.082}_{-0.061}$
ϖ	Parallax(mas)	12.941 ± 0.039
d	Distance (pc)	77.27 ± 0.23
Wavelength Parameters:		TESS
u_1	Linear limb-darkening coeff	0.262 ± 0.019
u_2	Quadratic limb-darkening coeff	0.289 ± 0.022

companion detections (Howell et al. 2011). The observations were carried out on 2022 September 14. No apparent sign of a stellar companion was detected from the imaging data down to the sensitivity limit of the instrument. Figure 4 shows our 562 nm and 832nm contrast curve results and our reconstructed speckle image. Specifically, we find that HD 17156 is a single star with no close companion brighter than 5–8.5 mag within the 5σ contrast and angular limits achieved ($0''.02$ – $1''.2$). The angular limits, at the distance of HD 17156 ($d = 78$ pc; see Table 3), correspond to spatial limits of 1.6 au to 94 au. These results are consistent with those from Adams et al. (2013), who did not detect any stellar companions within the angular range

Table 4
HD 17156 Planetary Parameters

Parameter	Units	Values
P	Period (days).....	21.2164294 ± 0.0000061
R_p	Radius (R_J).....	$1.094^{+0.031}_{-0.030}$
M_p	Mass (M_J).....	3.26 ± 0.11
T_C	Time of conjunction (BJD _{TDB}).....	$2458809.07037 \pm 0.00021$
a	Semimajor axis (AU).....	0.1632 ± 0.0027
i	Inclination (Degrees).....	$86.51^{+0.37}_{-0.34}$
e	Eccentricity	$0.6772^{+0.0045}_{-0.0044}$
ω_*	Argument of periastron (Degrees).....	122.06 ± 0.37
T_{eq}	Equilibrium temperature (K).....	888^{+12}_{-11}
τ_{circ}	Tidal circularization timescale (Gyr).....	$20.7^{+3.8}_{-3.2}$
K	RV semi-amplitude (m s^{-1}).....	$274.5^{+2.5}_{-2.3}$
R_p/R_*	Radius of planet in stellar radii	$0.07412^{+0.00039}_{-0.00040}$
a/R_*	Semimajor axis in stellar radii	$23.11^{+0.56}_{-0.53}$
δ	$(R_p/R_*)^2$	$0.005493^{+0.000058}_{-0.000059}$
δ_{TESS}	Transit depth in TESS (fraction).....	0.006085 ± 0.000055
τ	Ingress/egress transit duration (days).....	$0.01162^{+0.00062}_{-0.00060}$
T_{14}	Total transit duration (days).....	$0.13127^{+0.00066}_{-0.00064}$
T_{FWHM}	FWHM transit duration (days).....	$0.11965^{+0.00036}_{-0.00035}$
b	Transit impact parameter	$0.484^{+0.035}_{-0.041}$
b_S	Eclipse impact parameter	$1.79^{+0.13}_{-0.15}$
ρ_p	Density (cgs).....	$3.08^{+0.26}_{-0.23}$
$\log g_p$	Surface gravity	3.829 ± 0.024
Θ	Safronov number	0.757 ± 0.021
$\langle F \rangle$	Incident flux ($10^9 \text{ erg s}^{-1} \text{ cm}^{-2}$).....	$0.0937^{+0.0053}_{-0.0044}$
T_p	Time of periastron (BJD _{TDB}).....	$2458788.1332^{+0.0056}_{-0.0055}$
T_S	Time of eclipse (BJD _{TDB}).....	$2458813.946^{+0.080}_{-0.084}$
V_c/V_e	$0.4675^{+0.0034}_{-0.0035}$
$e \cos \omega_*$	$-0.3595^{+0.0051}_{-0.0053}$
$e \sin \omega_*$	$0.5739^{+0.0035}_{-0.0034}$
$M_p \sin i$	Minimum mass (M_J).....	3.26 ± 0.11
M_p/M_*	Mass ratio	$0.002425^{+0.000043}_{-0.000041}$
d/R_*	Separation at midtransit	$7.95^{+0.24}_{-0.23}$
$\dot{\gamma}$	RV slope ¹ ($\text{m s}^{-1}/\text{day}$).....	-0.00074 ± 0.00034
Telescope Parameters:		HIRES
γ_{rel}	Relative RV offset ¹ (m s^{-1}).....	-11.64 ± 0.80
σ_J	RV jitter (m s^{-1}).....	$4.26^{+0.45}_{-0.40}$
σ_J^2	RV jitter variance	$18.1^{+4.1}_{-3.2}$

Note.

¹ Reference epoch = 2456802.342883

of $0''.5\text{--}4''.0$ (39–312 au). The implications of these results are discussed further in Section 4.

3. Results

The data described in Section 2 provide a solid foundation from which to construct a thorough analysis and characterization of the star, planet, and other possible companions within the system.

3.1. Extraction of System Parameters

Here we provide new and updated properties for the HD 17156 system. The extraction of stellar and planetary properties was largely performed using the EXOFASTV2 tool¹⁴, described in detail by Eastman et al. (2013, 2019). We followed a similar application of EXOFASTV2 to that used by Kane et al. (2020), while applying noise floors to the stellar effective

temperature and bolometric flux (Tayar et al. 2022). We derived stellar properties for our sample by applying the SPECMATCH (Petigura et al. 2015) and ISOCCLASSIFY (Huber et al. 2017) software packages to the template Keck-HIRES spectra of our stars. SPECMATCH takes an optical stellar spectrum as input, and by interpolating over a grid of template spectra with known associated stellar properties, returns three spectral properties and uncertainties. We updated the normal prior on parallax to those provided by the third data release of the Gaia mission (Gaia Collaboration et al. 2021), including the corrections provided by Lindegren et al. (2021). Convergence for the global fit to the transit and RV data was assessed using the default EXOFASTV2 statistics of T_z (Ford 2006), the number of independent draws of the underlying posterior probability distribution (convergence for $T_z > 1000$ for each parameter), and the Gelman–Rubin statistic (GR; Gelman & Rubin 1992), where convergence is achieved for $\text{GR} < 1.01$ for each parameter.

¹⁴ <https://github.com/jdeast/EXOFASTv2>

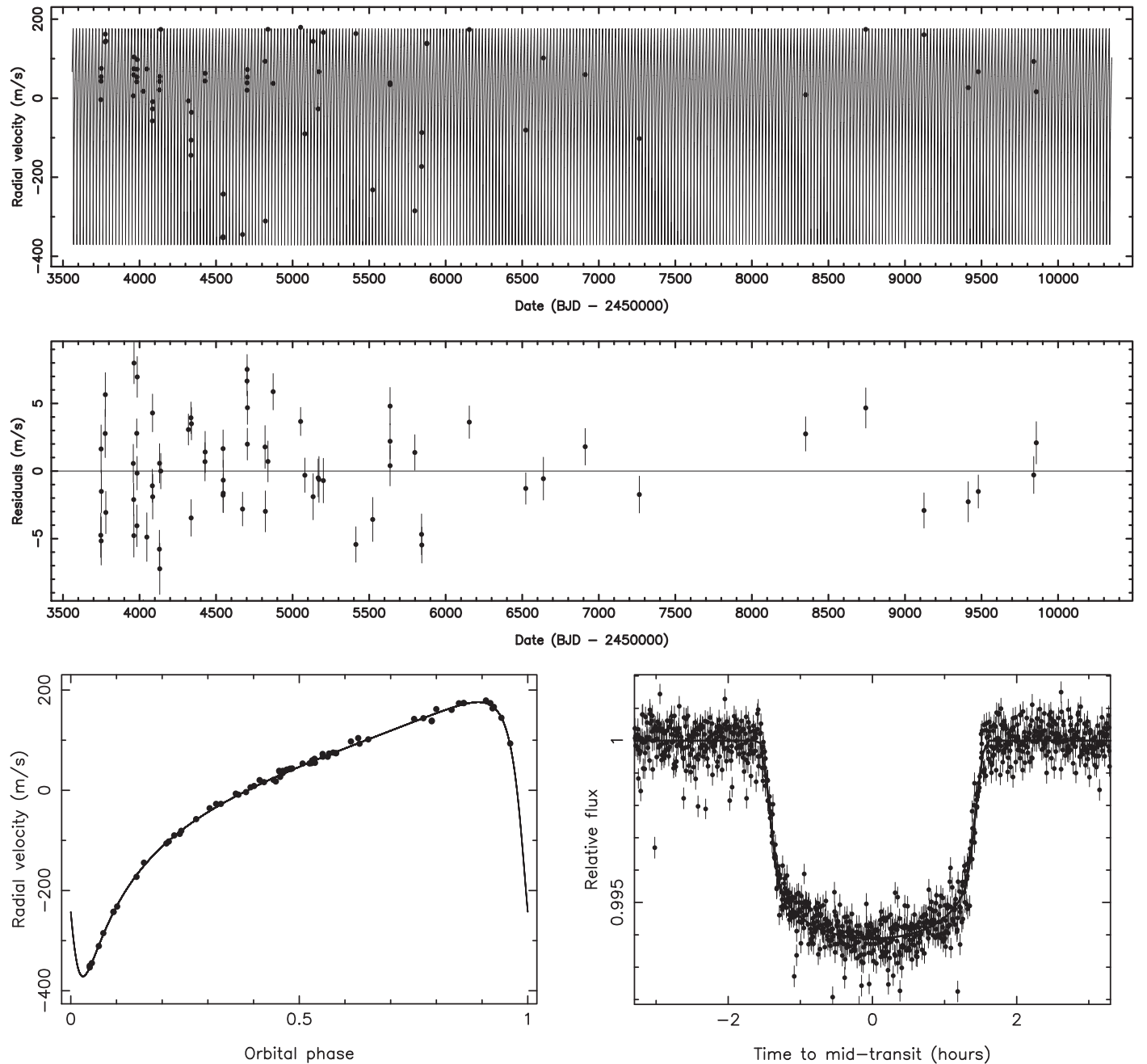


Figure 5. RV and TESS photometric data for HD 17156. Top panel: all Keck/HIRES RV data, spanning a total period of ~ 17 yr, along with the best-fit model after applying the EXOFAST fits described in Section 3.1. Middle panel: residuals from the best-fit model applied to the RV data. Bottom-left panel: RV data folded on the orbital period of the known planet. Bottom-right panel: transit fit from the EXOFAST analysis to the combined TESS photometry described in Section 2.1.2, where all five transits have been folded on the planetary orbital period.

The derived stellar parameters from the global EXOFASTV2 fit are shown in Table 3. In summary, HD 17156 is a G0 subgiant star, slightly more massive than the Sun, and with an age of ~ 3.3 Gyr. In addition to these parameters, SPECMATCH analysis provided a projected stellar rotational velocity of $v \sin i = 4.32 \pm 1.0 \text{ km s}^{-1}$. As described in Section 1, analysis of the R-M effect via RV data of the system during planetary transit revealed that the system exhibits a relatively small spin-orbit misalignment. Thus the projected stellar rotational velocity is a good approximation for the true rotational velocity, which predicts a rotation period of ~ 17.8 days, consistent with the above cited stellar age. As described in Section 2, we do not detect evidence of stellar

variability on short timescales, including any periodic signals near 17 days. However, the APT photometry (Section 2.1.1) indicates the presence of a ~ 10 yr photometric signature, possibly due to the the magnetic activity cycle of the host star (Strassmeier 2005; Dragomir et al. 2012).

The planetary parameters derived from the EXOFASTV2 analysis are provided in Table 4. There are numerous items of note regarding the data in this table. Timing information are shown with the subscript “TDB,” the Barycentric Dynamical Time, which includes relativistic corrections that move the origin to the barycenter. The revised orbital period has exceptionally small uncertainties similar to that determined by Ivshina & Winn (2022), though our fit includes more

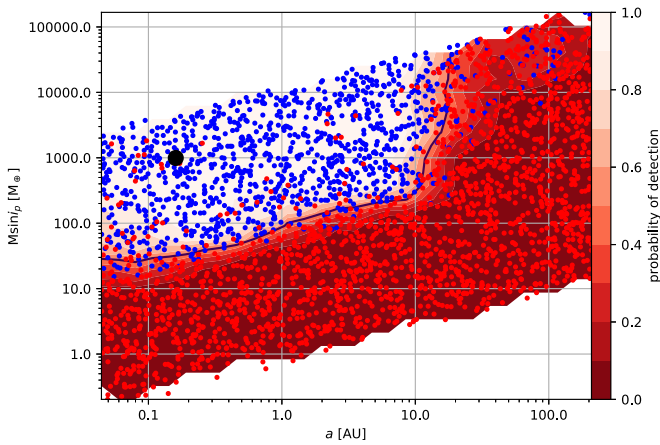


Figure 6. Injection-recovery results that determine the sensitivity of the HD 17156 RV data to planetary signatures as a function of planetary mass ($M_p \sin i$) and semimajor axis (a). The large black dot indicates the mass and semimajor axis of the known planet. The blue dots represent injected planetary signatures that were successfully recovered and the red dots represent those that were not recovered. The color scale corresponding to the probability contours of detecting a planet of a given mass and semimajor axis is shown on the right vertical axis.

transits and the combination with the RV data. The equilibrium temperature (~ 888 K) is calculated at the semimajor axis of the orbit and assumes no albedo and perfect heat redistribution (Kane & Gelino 2011). Using these same assumptions, the equilibrium temperature approaches 1600 K during periastron passage. The eclipse impact parameter, b_s , is greater than unity, since the eccentricity and periastron argument of the orbit ensure that the planet does not pass directly behind the host star during superior conjunction. V_c/V_e is the velocity ratio of the planet between circular and eccentric orbit scenarios during inferior conjunction, indicating the significant reduction in transit duration caused by the orbital orientation relative to the line of sight.

The best-fit RV and transit models are shown in Figure 5, along with their associated data. The top panel shows all of the Keck/HIRES RV data utilized in this analysis over the full span of ~ 17 yr. The uncertainties are shown in the plot, but the median RV uncertainty of 1.415 m s^{-1} (see Section 2.2) is small compared with the RV semi-amplitude of 274.5 m s^{-1} (see Table 4). The middle panel shows the residuals from the best-fit model applied to the RV data. The bottom-left panel of Figure 5 shows the RV data folded on the orbital period provided in Table 4. The bottom-right panel shows the TESS photometry from the four sectors described in Section 2.1.2 folded on the transit midpoint, along with the best-fit transit model.

3.2. Limits on Additional Planets

The various data sources described in Section 2 provide a compelling means through which to quantify the presence of other possible companions within the HD 17156 system. For example, as stated in Section 2.1.2, the rms scatter of the TESS photometry is 380 ppm over the sectors for which the target was observed. Adopting the stellar parameters provided in Table 3, this is equivalent to the transit depth of a $0.3 R_J$ planet. The transit of such an additional planet, assuming the orbital inclination is appropriately aligned, would thus have been detected within the TESS photometry if it occurred during the observed sectors. The imaging data (Section 2.3) demonstrate that there are unlikely to be stellar companions within the

system, and imaging possible planets rely on a correct assessment of their eccentricity (Kane 2013) and orbital ephemerides (Kane et al. 2018; Li et al. 2021).

The greatest constraints on additional planets arise from the RV data described in Section 2.2. Table 4 includes the linear slope of the RV data, incorporated as a free parameter in the overall fit to the data. The RV data exhibit a negligible slope, consistent with no further giant-planet companions within the system. To investigate this further, the RV data were used to perform an injection-recovery test that quantifies the completeness of the data for the detection of additional planetary signatures, as described by Howard & Fulton (2016). The method injects a variety of planet mass and semimajor axis signatures into the RV data, where the observation epochs and noise properties of the data are preserved. The injected signatures assume circular orbits and the fits to the resulting data sets are performed using the RadVel package (Fulton et al. 2018). The stellar mass from Table 3 was used for translating between the $M_p \sin i$ values and the RV semi-amplitude.

The injection-recovery results are shown in Figure 6 as a function of planet mass and semimajor axis, where the masses are provided in Earth masses (M_\oplus). The blue dots represent injected planets that were recovered and the red dots represent those that were not recovered. The shaded contours provide the probability of detection for the given planet mass and semimajor axis, indicated by color scale shown on the right vertical axis. The large black dot indicates the mass and semimajor axis of HD 17156b, which prominently lies within the regions of parameter space for which the RV data are sufficiently sensitive for a successful detection. These results establish that our RV data are sufficient to rule out additional planets within the system of Jupiter-mass planets within 10 au, and of Saturn-mass planets within 1 au. Planets below the detection limit may still be present in the system, including terrestrial planets at a wide range of separations from the host star, provided that they are not dynamically excluded by the gravitational influence of the known eccentric giant planet. Indeed, systems with a single eccentric planet can serve as excellent RV standards, due to the likely exclusion of terrestrial planets that would otherwise contribute to the RV error budget (Brewer et al. 2020).

4. Eccentricity Origin of the Known Planet

The relatively high eccentricity of HD 17156b poses an interesting question regarding the dynamical origin of the orbit, particularly as the calculated tidal circularization timescale of ~ 20.7 Gyr (see Table 4) is large compared with the estimated stellar age of ~ 3.3 Gyr (see Table 3). All of the data presented in this paper are consistent with a scenario in which there are no other companions within the HD 17156 system other than the star and planet. The RV data, described in Section 2.2 and Section 3.2, indicate that there are no other stellar or planetary companions down to the detection limit of the data. There may be additional terrestrial planets within several AU of the host star, but such planets are unlikely to have been a major dynamical contributor to the observed system. The speckle imaging data, described in Sections 2.3 and 3.2, are also consistent with a lack of stellar companions within the system, including wide separation orbits. This is in contrast to several other known systems that harbor highly-eccentric planets, such as HD 80606/HD 80607 (Naef et al. 2001; Liu et al. 2018) and HD 20781/HD 20782 (Jones et al. 2006; Mack et al. 2014;

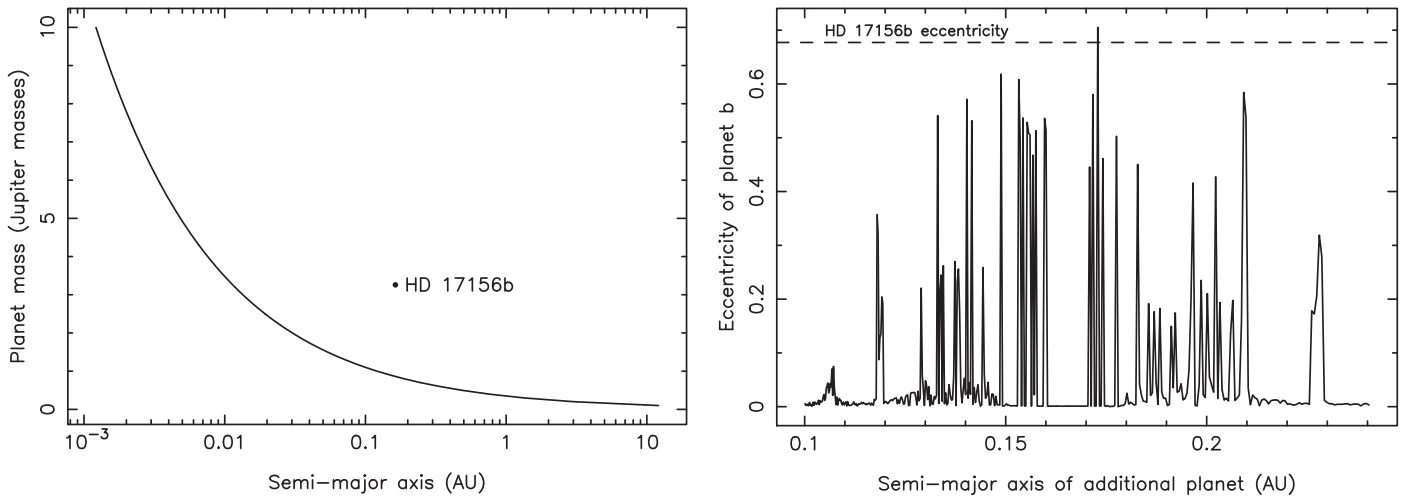


Figure 7. Left: the mass and semimajor axis of an additional planet in a circular orbit whose angular momentum equals the angular momentum deficit (AMD) for the HD 17156 system. The dot indicated the known mass and semimajor axis of HD 17156b. Right: eccentricity of HD 17156b as a function of the semimajor axis for the additional planet. The horizontal dashed line indicated the current eccentricity of HD 17156b.

Kane et al. 2016). Such binary systems present opportunities for orbital excitation of giant planets via gravitational interaction with the binary star companion during times of close approach (Malmberg & Davies 2009; Quarles et al. 2018). In the absence of stellar companions, as is the case for HD 17156, planet–planet scattering as the source of high eccentricity is a possible alternate scenario (Chatterjee et al. 2008; Ford & Rasio 2008; Mustill et al. 2017; Carrera et al. 2019).

To investigate planet–planet scattering scenarios for the system, we calculated the angular momentum deficit (AMD) for the system (Laskar 1997). The AMD describes the difference in total angular momentum between the eccentric orbits present within a system and equivalent circular orbits. The AMD thus may indicate lost angular momentum through planet ejection scenarios, and may also be used as an indicator of long-term planetary system stability (Laskar & Petit 2017; He et al. 2020). The AMD for the HD 17156 system is 3.33×10^{42} kg m²/s, which is approximately twice the orbital angular momentum of Uranus. We calculated a range of masses and semimajor axis values for a planet in a circular orbit that would have an angular momentum equivalent to the AMD of the HD 17156 system, the results of which are plotted in the left panel of Figure 7, along with the location of HD 17156b. These masses and semimajor axes encompass a broad range of values, and only a small subset of this full range are expected to result in significant planet–planet interactions.

We conducted hundreds of dynamical simulations via N -body integrations using the Mercury Integrator Package (Chambers 1999). The simulations adopted a time resolution of 0.1 days and used a hybrid symplectic/Bulirsch–Stoer integrator with a Jacobi coordinate system to provide increased accuracy for close encounters (Wisdom & Holman 1991; Wisdom 2006). We used the parameters for the known planet HD 17156b, shown in Table 4, but reduced the orbital eccentricity to zero. An additional planet was placed in a circular orbit in the semimajor axis range of 0.1–1.0 au with a mass dictated by the AMD calculations shown in the left panel of Figure 7. These system architectures were used as input for the dynamical simulations, each of which were executed for a total duration of 10^6 yr, equivalent to 1.72×10^7 orbits of

HD 17156b. For each simulation, the final eccentricity of HD 17156b was recorded.

The results of these simulations are represented in the right panel of Figure 7, which plots the semimajor axis of the additional planet and the final eccentricity of planet b. The horizontal dashed line indicates the current eccentricity of HD 17156b, $e = 0.6772$, as shown in Table 4. The majority of simulation cases result either in negligible interactions between the planets, or the additional planet being lost to the gravitational well of the host star. The spikes in eccentricity are the result of planet–planet scattering events in which the additional planet is ejected from the system, transferring significant angular momentum to the remaining planet. In all such cases, the remaining planet is HD 17156b, since it is substantially more massive than the additional planet, as seen in the left panel of Figure 7. The outcome of one simulation produced an eccentricity for HD 17156b of 0.7, slightly higher than its present value, caused by an additional planet with a mass of $0.84 M_J$ and semimajor axis of 0.173 au. This demonstrates the viability of the planet–planet scattering scenario as the source of the HD 17156b eccentricity. Note that this investigation is intended as a first-order study of possible planet–planet scattering scenarios, ignoring factors such as interactions with the disk during formation (Clement et al. 2021), and further planets that may have participated in the dynamical evolution of the system.

5. Conclusions

Planetary system architectures are at the forefront of exoplanetary science investigations, enabled by the vast amount of statistical data that are provided by discoveries over recent decades. The origin of highly-eccentric planets, one of the first observed significant divergences from the solar system architecture, remains an active area of research. HD 17156b was a key exoplanet detection, since the discovery of its transit placed it in a separate category from the population of hot Jupiters that was starting to emerge. The subsequent data for the system reveal that the star does not appear to have stellar companions, and the only known planet is alone in the system down to the detection limit of the data, ruling out additional

Jupiter-mass planets within 10 au, and of Saturn-mass within 1 au.

Although there are numerous scenarios that may produce highly-eccentric orbits, such as disk interactions and encounters with a stellar binary, the evidence in this case points toward a possible planet–planet scattering event. Although the use of the AMD to evaluate such planet–planet scattering scenarios is a first-order investigation tool, it does reveal possible eccentricity progenitors. There are now many other similar transiting systems with eccentric orbits that have been detected, thanks largely to the discoveries of the TESS mission. As this population continues to grow, a more exhaustive analysis of the eccentric planet population as a function of stellar and planetary multiplicity will provide further insights into the origins of highly-eccentric orbits.

The authors would like to thank Teo Močnik for discussions regarding HD 17156. G.W.H. acknowledges long-term support from NASA, NSF, Tennessee State University, and the State of Tennessee through its Centers of Excellence program. P.D. acknowledges support by a 51 Pegasi b Postdoctoral Fellowship from the Heising-Simons Foundation. T.F. acknowledges support from the University of California President's Postdoctoral Fellowship Program. We gratefully acknowledge the efforts and dedication of the Keck Observatory staff for support of HIRES and remote observing. We recognize and acknowledge the cultural role and reverence that the summit of Maunakea has within the indigenous Hawaiian community. We are deeply grateful to have the opportunity to conduct observations from this mountain. Observations in the paper also made use of the High-Resolution Imaging instrument 'Alopeke. 'Alopeke was funded by the NASA Exoplanet Exploration Program and built at the NASA Ames Research Center by Steve B. Howell, Nic Scott, Elliott P. Horch, and Emmett Quigley. 'Alopeke was mounted on the Gemini North telescope of the international Gemini Observatory, a program of NSF's NOIRLab, which is managed by the Association of Universities for Research in Astronomy (AURA) under a cooperative agreement with the National Science Foundation on behalf of the Gemini Observatory partnership: the National Science Foundation (United States), National Research Council (Canada), Agencia Nacional de Investigación y Desarrollo (Chile), Ministerio de Ciencia, Tecnología e Innovación (Argentina), Ministério da Ciência, Tecnologia, Inovações e Comunicações (Brazil), and Korea Astronomy and Space Science Institute (Republic of Korea). The results reported herein benefited from collaborations and/or information exchange within NASA's Nexus for Exoplanet System Science (NExSS) research coordination network sponsored by NASA's Science Mission Directorate.

Software: EXOFAST (Eastman et al. 2013, 2019), Mercury (Chambers 1999), RadVel (Fulton et al. 2018).

ORCID iDs

Stephen R. Kane <https://orcid.org/0000-0002-7084-0529>
 Michelle L. Hill <https://orcid.org/0000-0002-0139-4756>
 Paul A. Dalba <https://orcid.org/0000-0002-4297-5506>
 Tara Fetherolf <https://orcid.org/0000-0002-3551-279X>
 Gregory W. Henry <https://orcid.org/0000-0003-4155-8513>
 Sergio B. Fajardo-Acosta <https://orcid.org/0000-0001-9309-0102>
 Crystal L. Gnilká <https://orcid.org/0000-0003-2519-6161>

Andrew W. Howard <https://orcid.org/0000-0001-8638-0320>

Steve B. Howell <https://orcid.org/0000-0002-2532-2853>

Howard Isaacson <https://orcid.org/0000-0002-0531-1073>

References

- Adams, E. R., Dupree, A. K., Kulesa, C., & McCarthy, D. 2013, *AJ*, 146, 9
 Barbieri, M., Alonso, R., Desidera, S., et al. 2009, *A&A*, 503, 601
 Barbieri, M., Alonso, R., Laughlin, G., et al. 2007, *A&A*, 476, L13
 Barnes, J. W. 2007, *PASP*, 119, 986
 Brewer, J. M., Fischer, D. A., Blackman, R. T., et al. 2020, *AJ*, 160, 67
 Burke, C. J. 2008, *ApJ*, 679, 1566
 Butler, R. P., Marcy, G. W., Williams, E., et al. 1996, *PASP*, 108, 500
 Carrera, D., Raymond, S. N., & Davies, M. B. 2019, *A&A*, 629, L7
 Chambers, J. E. 1999, *MNRAS*, 304, 793
 Charbonneau, D., Brown, T. M., Latham, D. W., & Mayor, M. 2000, *ApJL*, 529, L45
 Chatterjee, S., Ford, E. B., Matsumura, S., & Rasio, F. A. 2008, *ApJ*, 686, 580
 Ciardi, D. R., Beichman, C. A., Horch, E. P., & Howell, S. B. 2015, *ApJ*, 805, 16
 Clement, M. S., Deienno, R., Kaib, N. A., et al. 2021, *Icar*, 367, 114556
 Cochran, W. D., Redfield, S., Endl, M., & Cochran, A. L. 2008, *ApJL*, 683, L59
 Dalba, P. A., Kane, S. R., Barclay, T., et al. 2019, *PASP*, 131, 034401
 Dalba, P. A., Kane, S. R., Li, Z., et al. 2021, *AJ*, 162, 154
 Dawson, R. I., & Johnson, J. A. 2012, *ApJ*, 756, 122
 de Wit, J., Lewis, N. K., Langton, J., et al. 2016, *ApJL*, 820, L33
 Dragomir, D., Kane, S. R., Henry, G. W., et al. 2012, *ApJ*, 754, 37
 Eastman, J., Gaudi, B. S., & Agol, E. 2013, *PASP*, 125, 83
 Eastman, J. D., Rodriguez, J. E., Agol, E., et al. 2019, arXiv:1907.09480
 Fetherolf, T., Pepper, J., Simpson, E., et al. 2022, arXiv:2208.11721
 Fischer, D. A., Vogt, S. S., Marcy, G. W., et al. 2007, *ApJ*, 669, 1336
 Ford, E. B. 2006, *ApJ*, 642, 505
 Ford, E. B. 2014, *PNAS*, 111, 12616
 Ford, E. B., & Rasio, F. A. 2008, *ApJ*, 686, 621
 Fulton, B. J., Petigura, E. A., Blunt, S., & Sinukoff, E. 2018, *PASP*, 130, 044504
 Fulton, B. J., Rosenthal, L. J., Hirsch, L. A., et al. 2021, *ApJS*, 255, 14
 Gelman, A., & Rubin, D. B. 1992, *StatSci*, 7, 457
 Georgakarakos, N., Eggl, S., & Dobbs-Dixon, I. 2018, *ApJ*, 856, 155
 Gilliland, R. L., McCullough, P. R., Nelan, E. P., et al. 2011, *ApJ*, 726, 2
 Gillon, M., Triaud, A. H. M. J., Mayor, M., et al. 2008, *A&A*, 485, 871
 Gaia Collaboration, Brown, A. G. A., Vallenari, A., et al. 2021, *A&A*, 649, A1
 He, M. Y., Ford, E. B., Ragozzine, D., & Carrera, D. 2020, *AJ*, 160, 276
 Henry, G. W. 1999, *PASP*, 111, 845
 Henry, G. W., Marcy, G. W., Butler, R. P., & Vogt, S. S. 2000, *ApJL*, 529, L41
 Hill, M. L., Kane, S. R., Seperuelo Duarte, E., et al. 2018, *ApJ*, 860, 67
 Howard, A. W., & Fulton, B. J. 2016, *PASP*, 128, 114401
 Howard, A. W., Johnson, J. A., Marcy, G. W., et al. 2009, *ApJ*, 696, 75
 Howell, S. B., Everett, M. E., Sherry, W., Horch, E., & Ciardi, D. R. 2011, *AJ*, 142, 19
 Huber, D., Zinn, J., Bojsen-Hansen, M., et al. 2017, *ApJ*, 844, 102
 Irwin, J., Charbonneau, D., Nutzman, P., et al. 2008, *ApJ*, 681, 636
 Ivshina, E. S., & Winn, J. N. 2022, *ApJS*, 259, 62
 Jones, H. R. A., Butler, R. P., Tinney, C. G., et al. 2006, *MNRAS*, 369, 249
 Jurić, M., & Tremaine, S. 2008, *ApJ*, 686, 603
 Kane, S. R. 2007, *MNRAS*, 380, 1488
 Kane, S. R. 2013, *ApJ*, 766, 10
 Kane, S. R., Arney, G. N., Byrne, P. K., et al. 2021a, *JGRE*, 126, e06643
 Kane, S. R., Bean, J. L., Campante, T. L., et al. 2021b, *PASP*, 133, 014402
 Kane, S. R., & Blunt, S. 2019, *AJ*, 158, 209
 Kane, S. R., Ciardi, D. R., Gelino, D. M., & von Braun, K. 2012, *MNRAS*, 425, 757
 Kane, S. R., & Gelino, D. M. 2011, *ApJ*, 741, 52
 Kane, S. R., & Gelino, D. M. 2012, *AsBio*, 12, 940
 Kane, S. R., Mahadevan, S., von Braun, K., Laughlin, G., & Ciardi, D. R. 2009, *PASP*, 121, 1386
 Kane, S. R., Meshkat, T., & Turnbull, M. C. 2018, *AJ*, 156, 267
 Kane, S. R., & Raymond, S. N. 2014, *ApJ*, 784, 104
 Kane, S. R., & von Braun, K. 2008, *ApJ*, 689, 492
 Kane, S. R., & von Braun, K. 2009, *PASP*, 121, 1096
 Kane, S. R., Wittenmyer, R. A., Hinkel, N. R., et al. 2016, *ApJ*, 821, 65
 Kane, S. R., Yalçinkaya, S., Osborn, H. P., et al. 2020, *AJ*, 160, 129
 Kataria, T., Showman, A. P., Lewis, N. K., et al. 2013, *ApJ*, 767, 76

- Laskar, J. 1997, *A&A*, **317**, L75
- Laskar, J., & Petit, A. C. 2017, *A&A*, **605**, A72
- Laughlin, G., Deming, D., Langton, J., et al. 2009, *Natur*, **457**, 562
- Lewis, N. K., Knutson, H. A., Showman, A. P., et al. 2013, *ApJ*, **766**, 95
- Li, Z., Hildebrandt, S. R., Kane, S. R., et al. 2021, *AJ*, **162**, 9
- Lindgren, L., Bastian, U., Biermann, M., et al. 2021, *A&A*, **649**, A4
- Liu, F., Yong, D., Asplund, M., et al. 2018, *A&A*, **614**, A138
- Lomb, N. R. 1976, *Ap&SS*, **39**, 447
- Mack, C. E. I., Schuler, S. C., Stassun, K. G., & Norris, J. 2014, *ApJ*, **787**, 98
- Maggio, A., Pillitteri, I., Scandariato, G., et al. 2015, *ApJL*, **811**, L2
- Malmberg, D., & Davies, M. B. 2009, *MNRAS*, **394**, L26
- Marcy, G. W., & Butler, R. P. 1992, *PASP*, **104**, 270
- Matson, R. A., Howell, S. B., Horch, E. P., & Everett, M. E. 2018, *AJ*, **156**, 31
- Mayorga, L. C., Robinson, T. D., Marley, M. S., May, E. M., & Stevenson, K. B. 2021, *ApJ*, **915**, 41
- Mustill, A. J., Davies, M. B., & Johansen, A. 2017, *MNRAS*, **468**, 3000
- Naef, D., Latham, D. W., Mayor, M., et al. 2001, *A&A*, **375**, L27
- Narita, N., Hirano, T., Sato, B., et al. 2009, *PASJ*, **61**, 991
- Narita, N., Sato, B., Ohshima, O., & Winn, J. N. 2008, *PASJ*, **60**, L1
- Nutzman, P., Gilliland, R. L., McCullough, P. R., et al. 2011, *ApJ*, **726**, 3
- Pepper, J., Kane, S. R., Rodriguez, J. E., et al. 2020, *AJ*, **159**, 243
- Petigura, E. A., Schlieder, J. E., Crossfield, I. J. M., et al. 2015, *ApJ*, **811**, 102
- Quarles, B., Lissauer, J. J., & Kaib, N. 2018, *AJ*, **155**, 64
- Ricker, G. R., Winn, J. N., Vanderspek, R., et al. 2015, *JATIS*, **1**, 014003
- Rosenthal, L. J., Fulton, B. J., Hirsch, L. A., et al. 2021, *ApJS*, **255**, 8
- Rosenthal, L. J., Knutson, H. A., Chachan, Y., et al. 2022, *ApJS*, **262**, 1
- Sánchez, M. B., de Elía, G. C., & Darriba, L. A. 2018, *MNRAS*, **481**, 1281
- Scargle, J. D. 1982, *ApJ*, **263**, 835
- Scott, N. J., Howell, S. B., Gnilka, C. L., et al. 2021, *FrASS*, **8**, 138
- Shen, Y., & Turner, E. L. 2008, *ApJ*, **685**, 553
- Southworth, J. 2011, *MNRAS*, **417**, 2166
- Strassmeier, K. G. 2005, *AN*, **326**, 269
- Tayar, J., Claytor, Z. R., Huber, D., & van Saders, J. 2022, *ApJ*, **927**, 31
- Valenti, J. A., Butler, R. P., & Marcy, G. W. 1995, *PASP*, **107**, 966
- Van Eylen, V., & Albrecht, S. 2015, *ApJ*, **808**, 126
- Vanderburg, A., & Johnson, J. A. 2014, *PASP*, **126**, 948
- Vogt, S. S., Allen, S. L., Bigelow, B. C., et al. 1994, *Proc. SPIE*, **2198**, 362
- Winn, J. N., & Fabrycky, D. C. 2015, *ARA&A*, **53**, 409
- Winn, J. N., Holman, M. J., Henry, G. W., et al. 2009, *ApJ*, **693**, 794
- Wisdom, J. 2006, *AJ*, **131**, 2294
- Wisdom, J., & Holman, M. 1991, *AJ*, **102**, 1528